

Modellization of hydraulic fracturing of porous materials¹

F. Tzschichholz¹ & M. Wangen²

¹ *Department of Physics, Norwegian University of Science and Technology, N-7034 Trondheim, Norway*

EMail: frank@ica1.uni-stuttgart.de

² *Institute for Energy Technology, N-2007 Kjeller, Norway*

EMail: magnus@ife.no

Abstract

We review microstructural fracture growth models suitable for the study of hydraulic fracture processes in disordered porous materials and present some basic results. It is shown that microstructural models exhibit certain similarities to corresponding theories of continua. These similarities are most easily demonstrated for simple crack geometries, i.e., straight cracks (finite size scalings). However, there exist even scaling relations which are completely independent of the particular employed crack structure. Furthermore it is demonstrated that disorder in cohesive/flow properties can influence the crack growth and the resulting fracture geometry in an essential way.

1 Introduction

The classification and prediction of breaking processes within solid materials forms an extremely difficult problem in engineering science as well as in solid state physics. This is even true for brittle materials exhibiting the simplest rheological behavior, i.e. no remanent deformations. Continuum mechanical treatments of brittle solids based on Griffith's theory¹ are quite widespread and accepted in scientific papers, and have been relatively successful for practical and engineering purposes.² There are, however, a couple of problems being associated with classical fracture mechanics limiting its range of application. Certain restrictions arise from the assumption that the deformations can be conducted in a thermodynamical reversible manner. Connected to this is the basic assumption that the involved fracture processes are thermodynamically reversible too. This

¹Reference: Advances in Fracture Mechanics, *Fracture of Rock* ed. M. H. Alibadi, (WIT Press, Southampton, 1999), p.227-61.

is usually expressed by minimizing thermodynamic potentials with respect to crack/fracture growth, which is a perturbational scheme. The typical modelling situation is such that some governing field equations are describing the global state of the deformation (i.e. the free energy density) according to some boundary/loading conditions while the free surface energy *field* (intrinsic strength) is classically assumed to be a constant property throughout the solid material. The assumption of a constant intrinsic strength constitutes a quite strong idealization for most experimental situations because it eliminates the field nature of cohesive properties. The assumption of a constant theoretical strength is most easily justified for *homogeneous* materials, i.e., perfect single crystals. However, even for such classes of materials there exist certain limitations: a) the crystal's cohesion is in general non-isotropic (variation in crystal strength according to crystallographic directions) and b) the cohesion is subject of thermal influences (lattice vibrations) introducing thermal fluctuations into the problem.

The survey becomes more difficult for most solid materials of practical interest as they are frequently composite materials. Variations of cohesive properties occur already on macroscopic length scales comparable to those of the microstructural elements. There is *no* simple argument to replace the theoretical strengths of the isolated solid phases by some average effective strength in connection with fracture problems. This is because the fracture and its associated *natural geometry* advances on a microstructural level where the heterogeneity in grain orientation and strength is present. We mention this in order to illustrate that the assumption of constant cohesion/binding properties throughout a solid and therefore the representation employing a homogeneous continuum needs careful consideration.

The investigation of geometrical properties of irreversibly grown cracks in the presence of disorder has recently received considerable attention among physicists. Basic ideas go back to statistical physics, theory of phase transitions, scaling theory, selfsimilarity and self-organized criticality. These concepts are described in good standard books of condensed matter physics, i.e. Chaikin & Lubensky.³ Perhaps one of the most well studied phenomena exhibiting self-organized criticality is Diffusion Limited Aggregation (DLA), theoretically first implemented by Witten & Sander.⁴ Its outline is quite simple and it is well suited to exemplify geometrical selfsimilarity.

Particles being small enough to be subject to Brownian motion diffuse in a large gas or fluid reservoir. The particle concentration is assumed to be very low (infinite dilution), i.e., there are at each time step precisely one diffusing particle and one cluster where the diffusing particle is allowed to be attached to. If the diffusing particle touches the particle-cluster it sticks to it forever and a new diffusing particle is started far away from the cluster. The process is called diffusion limited because the particle diffusion is the rate limiting step in this reaction scheme. Figure 1 shows such a DLA cluster. The cluster has a dendritic structure

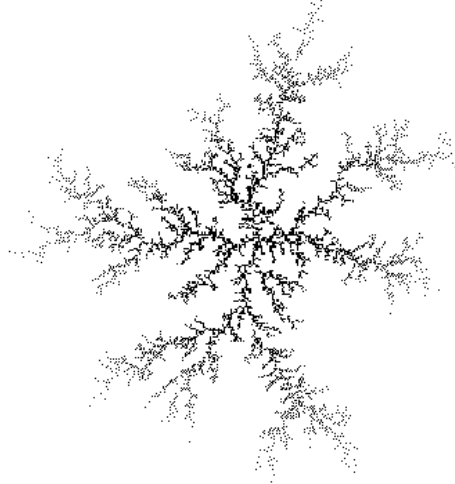


Figure 1: Selfsimilar DLA-Cluster in two dimensions consisting of 10^4 particles. The cluster grows outwards ‘absorbing’ diffusing particles coming from remote distances. The fractal dimension is $d_f = 1.71$. With courtesy of S. Schwarzer (numerical simulation).

exhibiting branches on all length scales between particle and cluster length scale. This supposes that the average number N of particles belonging to the cluster follows a power law in cluster radius R , i.e.,

$$N \sim R^{d_f}. \quad (1)$$

The exponent d_f is called the *fractal dimension* of the cluster. The value for d_f is in general always smaller equal the embedding dimension; in the above example $d_f = 1.71 < d = 2$. The physical meaning of a power law relation Eq.(1) is that the structure does not contain any natural length scale and that it looks similar to itself (selfsimilar) under a change of scale. The reader interested into concepts and applications of Fractals is referred to References 5 and 6. Nowadays it is widely believed that the value of the fractal dimension does only depend on the symmetries of the governing equations but not on particularities such as the particle shape or the employed discretisation scheme in numerical simulations. Deviations from scaling behavior are anticipated for systems of finite size.

The main interest in the DLA problem results from the fact that the governing equation is the Laplace equation being one of the most widespread and simplest equations in physics. A diffusing particle sticks with probability proportional to $\partial P / \partial n$ to the clustersurface with P being the solution of the diffusion equation. The sticking-probability is highest near the clusters extremities, so that

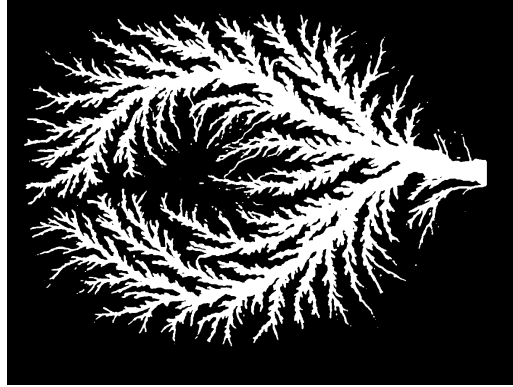


Figure 2: Lichtenberg figure in an epoxy plate. The figure shows the electrical discharge pattern towards a notch at the right side of the plate.⁹

the cluster is growing at a higher rate at the tips than in its interior. The tips screen the cluster interior to a certain amount leading to a diluted dendritic structure. Other examples belonging to the same *universality class* as DLA are the dielectric breakdown (DBM) (see Fig. 2), the viscous fingering (VF) (see Fig. 3a) and the Stefan problem of solidification.^{7,8} All these problems lead experimentally and numerically to similar geometrical patterns.

There has been considerable discussion whether fracture processes in presence of fluctuations would lead to DLA-like breakdown pattern too. The conducted investigations do, however, not support this idea in an unambiguous way. Rather the structure of the basic elastic equations (Lamé or Cosserat equations) *cannot* be reduced to a Laplace type equation even in limiting cases for the elastic constants. The experiments of Van Damme and collaborators on twodimensionally confined clay pastes display a sharp transition between DLA morphologies (viscous fingering, compare Fig. 3a) and the much more spiky and diluted hydraulic fractures, e.g. see Fig. 3b.

Further below we will present numerically obtained results mainly concerned with the problem of hydraulic fracturing of disordered materials in two dimensions.

We will first consider the case in which the model material contains only elastic interactions. We will investigate the cases of a constant injection (borehole-) pressure and of a constant fluid influx.

In a later chapter we consider a liquid saturated porous elastic material being fractured in a similar way. However, in such a case is the pressure distribution originating from the pore fluid flow directly coupled to the elastic equations.

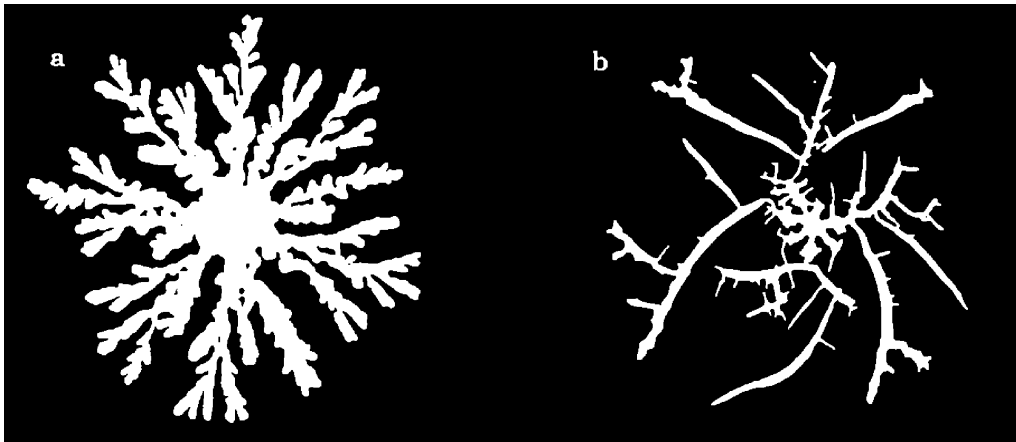


Figure 3: Fractal structures obtained after injecting water into Hele-Shaw cells containing clay pastes. (a) Viscous Fingering in a thin liquid paste (solid/liquid = 0.08). The fractal dimension is $d_f = 1.65$. (b) Hydraulic Fracturing in a thick paste (solid/liquid = 0.2). The fractal dimension is $d_f = 1.43$. Note that the fracture structure is more spiky than the viscous finger pattern. Both patterns were formed at the same constant injection pressure.¹⁰

2 The Model

In the following we will outline the employed model. We give a brief description of the basic elastic and flow equations. Thereafter we explain in detail the employed boundary conditions. After this we demonstrate how heterogeneous cohesive properties are taken into account. Finally we present the breaking rules which contain the physics of the considered breaking process.

2.1 Pore space

There are at least two different ways of implementing porosity numerically. In both cases certain microstructural elements (beams, plates or shells) will form a stress carrying elastic backbone. One can think, however, of two different realizations for the microstructural elements. The elements could be 'made' of a material which already follows the constitutive laws for porous materials, e.g. Biot's theory.¹¹ This would be most satisfying from a continuum mechanical point of view as long as no fracturing occurs. However, if *fracturing at the pore level* is to be taken into account the above mentioned approach does not suffice (or even becomes inconsistent) and a micromechanical approach must be employed. The pore space/volume has to be modelled explicitly in that case. We have focussed on the latter implementation: the microstructural elements follow the classical

constitutive equations of linear elasticity, and the pore space is viewed as the remaining vacant volume. The breaking of microstructural elements is associated with a coalescence of pore volume under question. Because the pore volume is modelled explicitly the couplings between elastic and flow interactions ought to be derived explicitly from the microstructural configuration.

In this paper we consider a two-dimensional model-microstructure laying on a square lattice with properties of the pore space (hydrostatic pressure field) defined on its dual lattice.¹²

2.2 Elastic equations

We consider the beam model (as defined in p. 232 of Ref. 13) on a two dimensional square lattice of linear size L . This model is preferable compared to Hookean spring models from a microstructural point of view because elastic beams due to their finite crosssection can be physically interpreted as fibers, while Hookean springs (having zero cross section) can not. In the two-dimensional beam model each of the lattice sites i carries three real variables: the two translational displacements x_i and y_i and a rotational angle φ_i in the xy-plane. Neighbouring sites are rigidly connected by elastic beams of length l . The beams are assumed to have the same quadratic cross section, $A = d^2$, and the same elastic behavior, governed by three material and geometry dependent constants $a = l/(Ed^2)$, $b = l/(Gd^2)$ and $c = 12l^3/(Ed^4)$ with E and G being the Young and shear moduli. With characteristic values for rock materials $E = 10^{11} \text{ Pa}$, $G = 4 \cdot 10^{10} \text{ Pa}$, $l = 10^{-5} \text{ m}$ and $d = 10^{-6} \text{ m}$ the above three constants become $a = 10^{-4} (\text{Pa m})^{-1}$, $b = 2.5 \cdot 10^{-4} (\text{Pa m})^{-1}$ and $c = 0.12 (\text{Pa m})^{-1}$. When a site is rotated ($\varphi_i \neq 0$) the beams bent accordingly always forming tangentially 90° angles with each other. In this way local momenta are taken into account. For a horizontal beam between sites i and j one has the longitudinal force acting at site j ,

$$F_j = \alpha(x_i - x_j), \quad (2)$$

the shear force

$$S_j = \beta(y_i - y_j) + \frac{\beta}{2}l(\varphi_i + \varphi_j), \quad (3)$$

and the flexural torque at site j ,

$$M_j = \frac{\beta}{2}l(y_i - y_j + l\varphi_j) + \delta l^2(\varphi_i - \varphi_j), \quad (4)$$

using $\alpha = 1/a$, $\beta = 1/(b + c/12)$ and $\delta = \beta(b/c + 1/3)$. The corresponding equations for vertical beams are similar. The outline of the beam network is displayed in Fig.4. We will not consider inertial or gravity forces, however, the flow of a

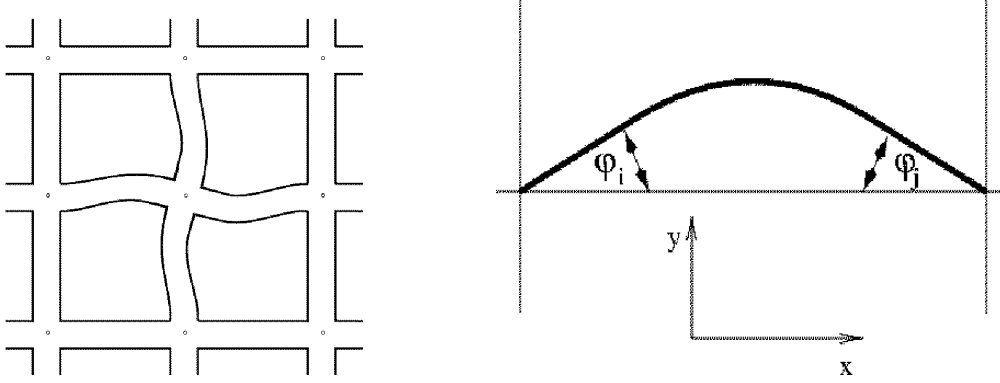


Figure 4: Schematic representation of the beam model (left) rotation of one site, (right) beam flexed due to the angles at its extremities.

pore fluid amounts in general to non-vanishing body forces. If there is a pressure drop $p_2 - p_1$ across a beam (pore wall) the resulting line force density can be replaced by a shear force dipole, $S = (p_1 - p_2)ld/2$, acting at both ends of that beam. This follows directly from the equilibrium conditions for beams. Hence the dipoles couple the pressure field in form of body forces to the mechanical equilibrium conditions.

In mechanical equilibrium the sum over all elastic and body forces (torques) acting on site j must vanish. Thus if the pressure field is known one can calculate the displacements.

To determine the hydrostatic pressure field one needs to consider flow equations.

2.3 Flow equations

The beams exhibit a typical length l and thickness d and the liquid saturated equilibrium pore volume is simply $(l - d)d^2$. This states explicitly the considered material to be a *binary* system, i.e. any volume element is either occupied by elastic material or by pore fluid. By varying the ratio of l/d different values for the volumetric porosity can be achieved (ranging from nearly zero to nearly one). In order to obtain most simplified flow equations, we make the following assumptions: a) the pore fluid is incompressible (which appears well justified for water) and b) the fluid velocity relative to the bulk is proportional to the gradient of the pressure field (Darcy's relation). The continuity equations for solid and liquid

mass density lead to the required pressure equation (in the continuum limit);

$$\operatorname{div}\left(\frac{k}{\mu} \operatorname{grad} p\right) = \frac{\partial}{\partial t} \operatorname{div} \mathbf{u}, \quad (5)$$

with p being the pressure, \mathbf{u} the displacement vector, k the mechanical permeability and μ the fluid viscosity. This equation is a Poisson equation for the pressure field for constant k and μ . The right hand side of Eq.(5) represents in general a time-dependent source term for the pressure field. It characterizes the local rate of relative volume change due to elastic deformations, and hence the net fluid flux itself. In general these net fluid fluxes will control the pressure field's time-evolution. However, in this work we will only consider the stationary case. The physical motivation for this is the observation, that the characteristic internal relaxation time $\tau = \mu/E$ for water-rock systems is typically of order 10^{-6} s. It appears justified to assume that the time periods between successive breaking events are much larger than the internal relaxation time τ , and hence that breaking events are triggered by stationary pressure and displacement distributions. In connection with Eq.(5) this implies to balance the net fluid flux for a given cell i to zero (Laplacian);

$$\frac{1}{\mu} \sum_j k_{ij}(p_i - p_j) + \text{boundary conditions} = 0. \quad (6)$$

Here k_{ij} denotes the local permeabilities across the beams (pore walls).

The pressure equation Eq.(6) is solved without referring to any mechanical properties, which is directly a consequence of explicitly dropping all dynamic terms. Its solution for given boundary conditions represents the body force under which the elastic equations, among their own boundary conditions, are solved. Formally the corresponding continuum problem is analogous to the standard problem of thermoelasticity¹⁴ which was already noted by Biot¹¹. From the resulting stresses/strains and breaking thresholds (see Sec.2.5) we then determine which element(s) are broken next.

Here we would just like to mention what happens to the pressure equations, when a beam is broken. Because the beams represent the pore walls, and because the fluid is assumed to be incompressible the pressure within a connected crack has to be constant. In this sense a crack is a macro-pore. Numerically this can be accomplished in different ways. We have chosen to set the permeabilities for broken beams very high, i.e. $k_{ij} = 10^9$. Hence the pressure drop along a crack is negligible small.

2.4 Boundary conditions

The results presented in this review are mainly for hydraulic fracturing conditions in impermeable^{15,16} and permeable¹⁷ materials. The only exception is Sec. 3 where we compare results for tensile and hydraulic loading configurations.¹⁸ The corresponding tensile boundary conditions are therefore discussed in Sec. 3.

Let us make few remarks about terminology. A boundary will be called ‘free’ if its normal stress component vanishes and will be called (hydrostatically) ‘loaded’ if the normal stress component follows some known non-zero stress distribution (von Neuman condition). A boundary is called ‘fixed’ or ‘clamped’ if the displacement values are assigned to the boundary (Dirichlet condition). A particularity in calculations are the sometimes employed ‘periodic’ boundary conditions for displacements/stresses. They enforce periodic displacement/stress field solutions. Periodic boundary conditions are especially useful in numerical calculations when the asymptotic behavior for infinite systems is of interest. We will encounter them in Sec. 3.

For most physical fracture problems the boundary conditions for the displacements are von Neuman conditions, or mixed boundary conditions. In presence of an additional flow equation boundary conditions for the fluid pressure field need to be specified. In our case homogeneous Dirichlet conditions are sufficient, i.e., the hydraulic crack pressure, p , and an equilibrium pressure, p_0 , for the external boundary.

In Sec. 3.2 and Sec. 4 we describe simulations where the hydraulic crack is ‘loaded’ and propagated by a constant crack pressure. The crack pressure does neither vary in space nor in time. The considered external boundaries (lattice edges) are either free or periodic.

A, for practical purposes, somewhat more realistic boundary condition propagating a hydraulic crack is a constant fluid injection rate, q_{in} . To keep things tractable we only consider an incompressible hydraulic fluid. The boundary condition for an impermeable crack, Sec. 5.1, is a particular case of the more general permeable crack boundary condition, see below. A constant fluid injection rate q_{in} corresponds to a certain driving pressure difference, $p - p_0$, where p denotes the hydraulic pressure within the crack and p_0 corresponds to an equilibrium pressure. We have used $p_0 = 0$. The hydraulic pressure does depend on q_{in} and the crack opening volume. For permeable cracks/materials p also depends on the hydraulic losses. In the following we will outline how to determine the hydraulic crack pressure p for given injection rate q_{in} and crack structure (contour) ∂V .

Because for an incompressible fluid the conservation of fluid mass directly implies a conservation of fluid volume, it is possible to formulate a continuity equation for the crack opening volume V ,

$$\frac{\partial V}{\partial t} + \int_{\partial V} \mathbf{v} \cdot d\mathbf{A} = q_{in}. \quad (7)$$

Here \mathbf{v} denotes the Darcy field integrated over the crack surface ∂V with surface element $d\mathbf{A}$. As source term appears the rate of injected (fluid) volume, q_{in} . Because the Darcy vectors are linear functionals of the pressure, $\mathbf{v} = -k/\mu \cdot \text{grad}p$, and the crack opening volume is a linear functional of displacements, $V = \int_{\partial V} \mathbf{u} \cdot d\mathbf{A}$, and because all considered equations are linear, a scaling of the form $p = \lambda p^*$ implies $\mathbf{v} = \lambda \mathbf{v}^*$, $\mathbf{u} = \lambda \mathbf{u}^*$ and $V = \lambda V^*$. Note that such a scaling is in general *impossible* if one considers Eq. (5) instead of the Laplacian, $\Delta p = 0$, as flow equation.

There exists an interesting application of Eq.(7) for undercritical, non-growing cracks. With V^* and \mathbf{v}^* depending *only* on the constant crack contour ∂V and crack pressure p^* one obtains a first order differential equation for the scaling factor $\lambda(t)$,

$$\frac{d\lambda}{dt} \cdot \int_{\partial V} \mathbf{u}^* \cdot d\mathbf{A} + \lambda \cdot \int_{\partial V} \mathbf{v}^* \cdot d\mathbf{A} = q_{in}, \quad (8)$$

with general solution,

$$\lambda(t) = \lambda_{\infty} + (\lambda_0 - \lambda_{\infty}) \cdot e^{-t/\tau}, \quad (9)$$

using

$$\lambda_{\infty} = \frac{q_{in}}{\int_{\partial V} \mathbf{v}^* \cdot d\mathbf{A}}, \quad \lambda_0 = \frac{p_0}{p^*}, \quad \tau = \frac{\int_{\partial V} \mathbf{u}^* \cdot d\mathbf{A}}{\int_{\partial V} \mathbf{v}^* \cdot d\mathbf{A}}. \quad (10)$$

The important point is that one can choose an *arbitrary* boundary value p^* within a calculation; the resulting $p = \lambda(t) \cdot p^*$ will be unique. However, one needs to calculate the contour integrals in Eq. (10) in order to do the rescaling.

The magnitude λ_{∞} does depend only on the injected fluid flux q_{in} and the total fluid flux through the crack contour. It does *not* depend on elastic properties. The typical time scale τ , above which the crack pressure and the crack opening volume tend to approach their asymptotic values, is given by the ratio of crack volume and fluid volume flux through the crack surface. It does *not* depend on the injected fluid flux. Again we would like to stress that the crack contour is assumed to be constant. However, Eq.(9) is quite general in the sense that all dependencies on the actual crack contour have been implicitly taken into account within the constants λ_{∞} and τ . Equation (9) should therefore hold for arbitrarily shaped cracks.

There are two limiting cases for the practical important situation $\lambda_0 \approx 0$. For large times, $t \gg \tau$, the scaling factor $\lambda(t) \rightarrow \lambda_{\infty}$ becomes constant and so do the crack pressure $p_{\infty} = q_{in}\tau \cdot (p^*/V^*)$ and the crack volume $V_{\infty} = q_{in}\tau$. The other limiting case is for small times, $t \ll \tau$, where the scaling factor becomes linear in time, $\lambda(t) = \frac{q_{in}}{V^*} \cdot t$ with corresponding pressure $p = q_{in} \frac{p^*}{V^*} \cdot t$ and volume $V = q_{in} \cdot t$. The latter case also holds for impermeable materials because $\lim_{k \rightarrow 0} \lambda(t) = q_{in}/V^* \cdot t$.

Equations (7) and (9) hold for *arbitrary* crack contours, i.e., branched or ramified cracks.

Equation 7 has a corresponding discrete update scheme. One just needs to be careful with the time derivative in Eq. (7) because the scaling factors λ are in general different before and after the time increment, Δt ,

$$\lambda(t + \Delta t) = \lambda(t) \cdot \left(1 - \frac{D^*}{V^*} \Delta t\right) + \frac{q_{in}}{V^*} \Delta t. \quad (11)$$

Here $D^* = \int_{\partial V} \mathbf{v}^* \cdot d\mathbf{A}$ and $V^* = \int_{\partial V} \mathbf{u}^* \cdot d\mathbf{A}$ denote the crack contour integrals/sums for the Darcy flows and displacements respectively, as obtained from the solution of the boundary value problem at time t with boundary value $p^* \neq 0$. As soon as the crack growths and its boundary changes one needs to recalculate the flow and the elastic equations in order to obtain the corresponding D^* and V^* . The ratio D^*/V^* being the inverse of a typical time will therefore change during the crack growth process.

We summarize:

1. Choose an initial crack boundary.
2. Set the initial value $\lambda(0)$, i.e., $\lambda(0) = 0$ (closed crack).
3. Solve the pressure equation Eq. (6) for an arbitrary hydraulic pressure p^* (boundary value for the current crack boundary).
4. Insert the corresponding pressure gradients into the elastic equations Eqs. (2)-(4) as inhomogeneities and solve the elastic equations.
5. Calculate from the obtained elastic solution the stress/force distribution σ^* .
6. Calculate from the elastic solution the crack opening volume V^* and from the pressure solution the total Darcy flux D^* .
7. Update λ according to Eq.(11).
8. Use the updated stresses/forces, $\sigma = \lambda\sigma^*$, in the breaking rule (see Sec. 2.6) and break the corresponding element(s).
9. Repeat steps 3-8 until a stopping criterion is fulfilled.

2.5 Heterogeneities

The problem of fracture processes in elastic media has undergone much attention in the last years, in particular the role of disorder in such processes.^{19–25} An important question of interest is how a variation in the *local* properties affects the *global* elastic properties in comparison to ideal homogeneous media. It was

recognized that elastic properties could considerably be changed and therefore interest was attracted how failure mechanisms like fracture, rupture or damage processes are influenced, changed or possibly controlled by disorder.

In the literature are two essentially different ways to take the disorder into account.¹³

The first possibility is to use exclusively the strain/stress field in order to calculate the probability for breaking a local constitutive element. This is known as stochastic disorder. Prominent *scalar* examples for this kind of disorder are known in the literature as Diffusion Limited Aggregation (DLA), Dielectric Breakdown or Viscous Fingering.^{7,8} We will present results for stochastic disorder in Sec. 4.

A second different kind of disorder is to initially assign a statically set of random values to certain material specific constants (structural disorder). Once these constants like strength, bending thresholds, elastic properties and others have been chosen the system behaves in a fully deterministic way. Corresponding results are presented in Sec. 5.

2.6 Breaking rules

Lattice fracture models like the beam model are spatially discrete. This is because one would like to have direct access to each constitutive elastic element. The medium is represented by a lattice and nearest neighbouring lattice points are connected by constitutive elastic elements called bonds. The bonds represent interactions not on an atomistic scale but rather on a mesoscopic scale, for example the elastic coupling between two adjacent grains where the grains themselves are linear elastic bodies. New features are the definitions of physically motivated "selection" and "breaking" rules for lattice bonds. Either a bond is broken according to some breaking rule and stays broken for the future or it remains intact and is further susceptible for the breaking process. The simulation ends when the elastic lattice fully breaks apart. Moreover, one has to define in the selection rule those bonds which could break in principle at a given stage of rupture. In single crack models only the surface bonds of the crack are allowed to break. However, in the many crack version in general all bonds are eligible. This allows in principle the nucleation of several microcracks in the system. We have used for our simulations the first kind of selection rule. In a recent published work²⁴ it was shown that if the disorder for the breaking thresholds is not too weak there are two different regimes in the macroscopic breaking characteristic. For small macroscopic strains first the weakest bonds are broken without leading to catastrophic failure. The breaking process is stable in this region and one has to increase the external applied stress in order to proceed breaking bonds. In finite systems however, this disorder controlled regime must end at the breaking point. The breaking process localizes, becomes unstable and a single large crack controls the entire breaking. It was shown that for different probability distributions of breaking thresholds

and different loading conditions two nontrivial possibly universal exponents are sufficient to rescale the macroscopic breakdown characteristics with respect to the system size. Breaking rules which determine the breaking conditions are crucial in lattice models because one has to put additional information about the fracture *mechanism* into the model which could not be obtained from elasticity theory. The employed breaking rules are described in the corresponding sections Sec. 3, Sec. 4, and Sec. 5.

3 Fracturing without disorder

We investigate both the case of uniaxial loading due to remote tensile forces and the loading due to a hydrostatic pressure acting from the interior on the crack surface. The former situation is typically encountered when a material is pulled at its outer faces, while the latter one can be found in engineering applications of hydraulic fracturing.²⁶ We will neglect inertial forces, assuming a sufficiently slow fracture process. The cohesive properties of the beams are considered to be homogeneous, i.e. the beams behave linear-elastic up to their theoretical strength F_{th} (cohesion force), above which they irreversibly break (zero elastic constants). At the beginning of each simulation we break one vertical beam located at the center of the lattice. This is the initial crack. Corresponding to the employed boundary conditions described below we calculate the internal force distribution F_{ij} of beams connecting sites i and j using a conjugate gradient method.²⁷ From this longitudinal forces we determine and break the most over stressed beam, i.e. the beam carrying the highest force, $F_{i_0j_0} = \max_{\{ij\}} F_{ij}$. The maximum force allows us to calculate a scaling factor $\lambda = F_{th}/F_{i_0j_0} = \sigma_{th}/\sigma_{i_0j_0}$ which in turn is used to determine the macroscopic breaking stress σ_c or breaking pressure P_c (measured in units of σ_{th}) necessary to fulfill the local fracture criterion $\sigma_{i_0j_0} = \sigma_{th}$. Such scaling is possible due to the linearity of the employed elastic equations. Breaking the beam connecting sites i_0 and j_0 destroys the balance of forces at those sites and one has to relax the system to its new equilibrium configuration. Then the above steps are repeated until the lattice breaks apart.

It is well known that the highest stress enhancement factors occur at the crack tips for the pressure as well as for the tensile problem. Because we consider only homogeneous cohesion forces the terms ‘most over stressed’ and ‘highest stress’ are equivalent and the cracks grow linear in direction of the highest local tensile force. In our case the direction of crack growth is the x-direction because of the uniaxiality of imposed boundary conditions, see below.

3.1 Tensile fracturing

To impose an external strain we attach at the bottom of the lattice a zeroth line on which for all sites $x_i = y_i = \varphi_i = 0$ are fixed, and on the top we attach

a $(L + 1)$ st line on which all sites have the same fixed values $x_i = \varphi_i = 0$ and $y_i = 1$. With this boundary conditions the external displacement in y-direction is fixed to unity (Dirichlet boundary conditions) and one can imagine them as being represented by rigid bars attached at the top and the bottom of the lattice. For the boundary conditions in x-direction we consider periodic as well as free lattice boundaries. The externally applied stress, σ_0 , necessary to maintain a unity displacement between the two rigid bars can be easily calculated by summing up all y_i displacements over the first line, $\sigma_0 = \frac{\alpha}{AL} \sum y_i$, where α is the longitudinal force constant, A the cross section of the beam and L the (dimensionless) lattice size. Employing the above defined scaling factor λ we express the externally applied breaking stress, σ_c , in the form,

$$\sigma_c = \lambda \sigma_0, \quad (12)$$

or in dimensionless form,

$$\frac{\sigma_c}{\sigma_{th}} = \frac{1}{F_{i_0 j_0}} \frac{\alpha}{L} \sum y_i. \quad (13)$$

With this notation the external breaking stress σ_c is just the stress necessary to yield the local breaking condition $\sigma_{i_0 j_0} = \sigma_{th}$.

We will use Eq.(13) for our finite-size scaling purposes. It expresses the breaking stress, measured in units of cohesion stress, in terms of the beam force $F_{i_0 j_0}$ at the ‘crack tip’ and the average force $\frac{\alpha}{L} \sum y_i$ on a beam due to the global unit displacement. In general both terms depend on the number of broken beams N (crack size) and on the lattice size L , see Sec. 3.3.1.

3.2 Hydraulic fracturing

Experimentally hydraulic fracturing is encountered when an incompressible fluid is injected under high pressure into an existing crack. The characteristics of this particular loading mode is that the loading of the crack only happens on the crack surface itself, but not on remote surfaces like in the case of tensile fracturing. Recently hydraulic fracturing has been numerically addressed by introducing for each broken beam a force dipole of strength F_0 simulating an inner pressure $P_0 = F_0/A$.^{15,16} In the present section we will follow this implementation. The basic assumptions are a) the pore fluid is highly compressible (gas), b) the permeability is negligible and c) the injected fluid is incompressible. Starting from one vertical broken beam (zero elastic constants, one vertical force dipole) we calculate the internal stress distribution F_{ij} using the conjugate gradient. Calculating the scaling factor λ as described above we determine and break the beam carrying the highest stress, $F_{i_0 j_0}$. Thereafter the lattice has to be relaxed again (now two broken beams, two force dipoles) and one repeats the above mentioned steps until the lattice breaks apart. The crack growth is single connected. As always the

two vertical beams in front of both crack tips are most overstressed and broken. Hence the existence of a connected path for the liquid is guaranteed.

We have performed calculations for free external boundaries in x- and y-direction as well as for periodic boundaries in x-direction and free boundaries in y-direction. As we only impose stresses the elastic solution (displacement field) is unique up to a general translation and rotation. Without restriction we therefore fix the displacement of an arbitrary lattice site to zero. Analogous to Eqs. (12) and (13) one has for the breaking pressure,

$$P_c = \lambda P_0, \quad (14)$$

and

$$\frac{P_c}{\sigma_{th}} = \frac{F_0}{F_{i_0 j_0}}, \quad (15)$$

respectively. It should be noted that σ_{th} is the tensile strength and not the compressional strength. In fact the stresses at the tips are tensile stresses as the crack is hydraulically opened.

We will use Eq. (15) for the finite-size scaling of the hydraulic problem.

3.3 Results

As explained in Sec. 3.1 and 3.2 we obtain from our simulations the macroscopic breaking stresses and pressures, $\sigma_c(N, L)$ and $P_c(N, L)$, measured in units of the theoretical strength σ_{th} , in terms of the number of broken beams N and the employed lattice sizes L . As we are interested in the finite-size scaling properties of the breaking stresses ($\Sigma_c = \sigma_c$) and pressures ($\Sigma_c = P_c$) we introduce two new functions, $\Psi(N)$ and $\Phi(N/L)$,

$$\Sigma_c(N, L) = \sigma_{th} \Psi(N) \Phi(N/L). \quad (16)$$

The function $\Phi(N/L)$ describes the finite-size corrections to the scaling $\Psi(N)$ between the breaking stress/pressure and the crack length for given boundary conditions in the infinite system. The quantity N/L is for our purposes the most suitable scaling variable as it represents the length of a linear crack measured in units of the employed lattice size. In general both functions, Ψ and Φ will depend on the employed boundary conditions. The dependence of the asymptotic scaling Ψ on employed boundary conditions appears to be contrary to what is expected from the theory of critical phenomena. In fact the asymptotic scalings Ψ for breaking stresses and pressures of continua without internal length scale are identical. However, as we will see below this is no longer necessarily true for systems with internal length scale. One obtains rather finite-size corrections originating from this scale which, depending on the employed boundary conditions, can result in very broad, non universal transient regions.

In order to show numerically that the finite-size scaling function $\Phi(N/L)$ exists, one needs to know (or to conjecture) the explicit form of $\Psi(N)$, i.e. the asymptotic behavior of Σ_c as $L \rightarrow \infty$.

We will access the latter information from simple continuum mechanical considerations of symmetric elasticity.

3.3.1 Tensile fracturing

Previous continuum mechanical scaling considerations have successfully been applied to fracture models. It has been shown¹⁸ that the breaking stress σ_c for tensile fracturing of a finite, periodic beam lattice follows very well the known ‘Tangent-Formula’ of fracture mechanics^{28,29},

$$\frac{\sigma_c}{\sigma_{th}} \sim N^{-1/2} \sqrt{\frac{N}{L} \cot \frac{\pi N}{2L}}. \quad (17)$$

By comparison with Eq. (16) we see that the asymptotic scaling for the breaking stress σ_c is given by $\Psi \sim N^{-1/2}$, a result that originally was found by Griffith. In Fig. 5 we show the finite-size scalings for the numerically obtained tensile breaking stresses (a) for free boundary conditions and (b) for periodic boundary conditions. For both curves the data collapse is quite acceptable. While for the periodic problem the finite-size correction $\Phi(N/L)$ follows Eq. (17)¹⁸, no analytical expression for Φ is known in the case of free boundary conditions. However, the differences for the breaking stresses at given values of N/L are less than $0.1\sigma_{th}$, see Fig. 5, and Eq. (17) represents a reasonably good approximation for finite solids for many practical purposes.

3.3.2 Hydraulic fracturing

In general analytical solutions of crack problems are difficult to obtain and even for two-dimensional problems in infinite, semi-infinite or periodic domains one is often faced with complicated integral equations. The reader interested in this is referred to Muskhelishvili³⁰ and Sneddon²⁹.

It has been shown analytically that the breaking pressure P_c of a semi-infinite two-dimensional continuum with periodic boundary conditions is given by Eq. (17) where one has to replace σ_c by P_c .²⁹ We show in Fig. 6 the analogous plot to Fig. 5 for the breaking pressure. One does not obtain a data collapse, indicating that $\Psi \sim N^{-1/2}$, see Eqs. (16) and (17), is *not* the scaling of the breaking pressure in the asymptotic limit of infinite lattices.

This result is somewhat unexpected, because the continuum limit predicts identical scaling relations for breaking stresses and pressures and on the other hand we find good agreement between lattice and continuum scalings for the tensile problem.

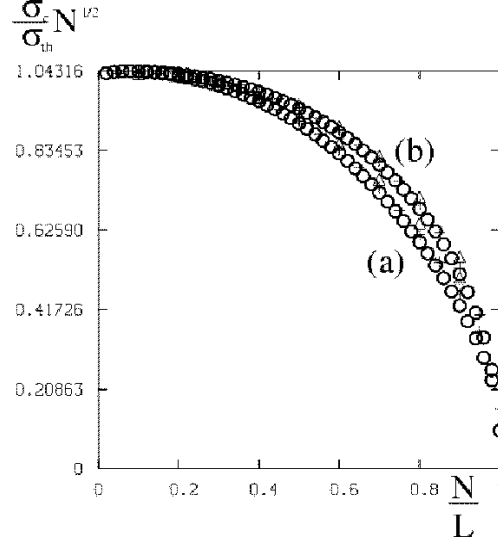


Figure 5: Finite-size scaling for the rescaled breaking stress $\sigma_c/\sigma_{th}N^{1/2}$ as a function of the rescaled crack length N/L , (a) for free boundaries in x-direction and (b) for periodic boundaries in x-direction. Lattice sizes: (\triangle) for $L = 20$, (+) for $L = 40$ and (\circ) for $L = 100$.¹⁸

However, the proposed model for hydraulic fracturing is defined on a lattice and not in a continuum. As lattices always show additional structure, higher order gradient terms of the continuum displacement field appear in the elastic solution, which have no counterparts in simple continua.^{31,32,33}

In the following we present an argument why the lattice finite-size scalings for the pressure and tensile problem are different.

In the tensile problem the loading forces are acting at the lattice boundaries *remote* to the stress free crack surfaces. Therefore local stresses close to the crack tips are carried through nearly the whole elastic volume. Contrary to this in the hydraulic problem loading only happens due to force dipoles acting at the crack surfaces *close* to the crack tips. One therefore might expect that the breaking pressures P_c show a more pronounced ‘(micro structure) lattice behavior’ than the breaking stresses σ_c . For very large cracks these differences should diminish as the discrete loading approaches a force density.

In order to extent a linear crack of length N in an infinite continuum one has to impose a breaking pressure $P_c \sim N^{-1/2}$. However, employing a *single double force* of magnitude F_c one finds, $F_c \sim N^{1/2}$ for the critical loading force (related Boussinesq problem).³⁴

We argue now that for a single crack in an infinite disk loaded by equidistant force dipoles the asymptotic scaling for Ψ is equivalent to that of an infinite lattice. Knowing Ψ we plot the finite-size scalings for the investigated lattices.

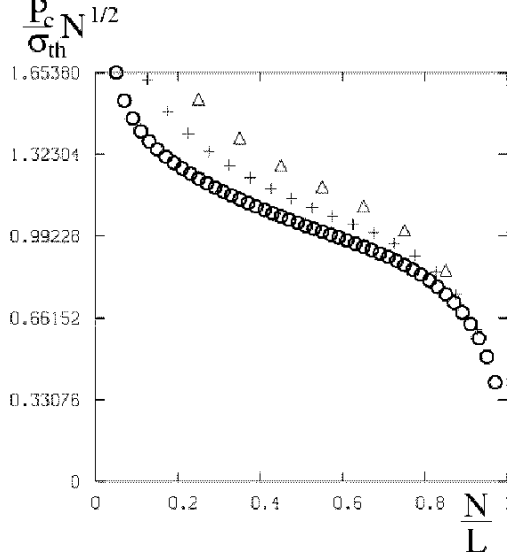


Figure 6: Plot of the rescaled breaking pressure $P_c/\sigma_{th}N^{1/2}$ as a function of the rescaled crack length N/L for periodic boundaries in x-direction. In contrast to Fig. 5 we do not find any data collapse, indicating that $\Psi(N) \sim N^{-1/2}$ in Eq. (16) is not the appropriate asymptotic expression for the breaking pressure. Lattice sizes: (\triangle) for $L = 20$, (+) for $L = 40$ and (\circ) for $L = 100$.¹⁸

The asymptotic continuum scaling for the breaking pressure (as calculated from equidistant force dipoles) is most easily obtained using the complex stress function of Westergaard.^{34,28} We find for the asymptotic scaling in an infinite disk,

$$\Psi(N) \approx \frac{\pi}{2} \frac{N^{1/2}}{1 + N f(N)}, \quad (18)$$

with

$$f(N) = \sum_{k=1}^{(N-1)/2} \frac{1}{\sqrt{(\frac{N+1}{2})^2 - k^2}}, \quad N \text{ odd}. \quad (19)$$

The sum $f(N)$ converges rapidly towards $\arcsin(\frac{N-1}{N+1})$ and for large N towards $\pi/2$. Hence in the limit of a large number of force dipoles we obtain the aforementioned asymptotic Griffith scaling for the breaking pressure, $P_c/\sigma_{th} = N^{-1/2}$.

In Fig. 7 we show the resulting finite-size scalings for the breaking pressure, based on Eqs. (16) and (18). In this plot a reasonable scaling is obtained, which proves our earlier statement that the asymptotic limits ($L \rightarrow \infty$) of the breaking pressures for continua and lattices are different.

Comparing Fig. 7 with Fig. 5 one also notes a significant deviation from the scaling form Eq. (17), demonstrating a modified correction to scaling behavior.

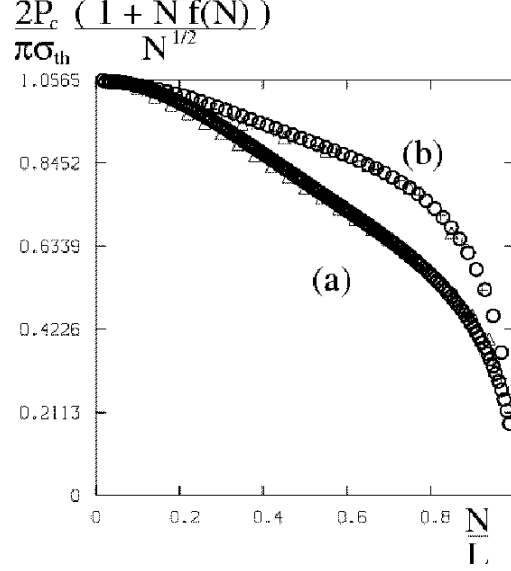


Figure 7: Finite-size scaling for the rescaled breaking pressure $P_c/\sigma_{th}\Psi^{-1}(N)$ with $\Psi^{-1}(N) = \frac{2}{\pi} \frac{1+N f(N)}{N^{1/2}}$, see Eq.(18), as a function of the rescaled crack length N/L ; (a) for free boundaries (Δ) : $L = 50$, (+) : $L = 100$, (\circ) : $L = 300$; (b) for periodic boundaries (Δ) : $L = 20$, (+) : $L = 40$, (\circ) : $L = 100$. Note the data collapses.¹⁸

4 Hydraulic Fracturing with stochastic disorder

We briefly discussed in the introduction, Sec. 1, Diffusion Limited Aggregation and its associated fractal aggregates. Essentially DLA clusters growth by adding one particle per “simulation step” to the clusters surface with a probability, p_{ij} , proportional to the local field gradient $|\nabla P|$ obtained from Laplace’s equation, $\Delta P = 0$. Similar considerations apply for the quasistatic growth of electrical discharge patterns, where an elementary discharge event is assumed to happen with a probability proportional to the local electrical field.⁴ Typically the boundary conditions are Dirichlet conditions for the external and the cluster surface.

There have been attempts in literature to generalize the DLA model in several ways. A main proposition was the introduction of a growth exponent, η , describing how strong the growth probabilities are correlated to the gradients, $p_{ij} \sim |\nabla P|^\eta$. For $\eta \rightarrow \infty$ the probability distribution becomes arbitrarily narrow (a delta peak) and the model is completely deterministic, i.e., the cluster grows *always* at the surface location of highest field gradient (current). The resulting structures are usually linear in two dimensions. The case $\eta = 1$ corresponds to fractal DLA cluster growth, as already mentioned above. For $\eta = 0$ the cluster growth is completely controlled by fluctuations and independent of the field

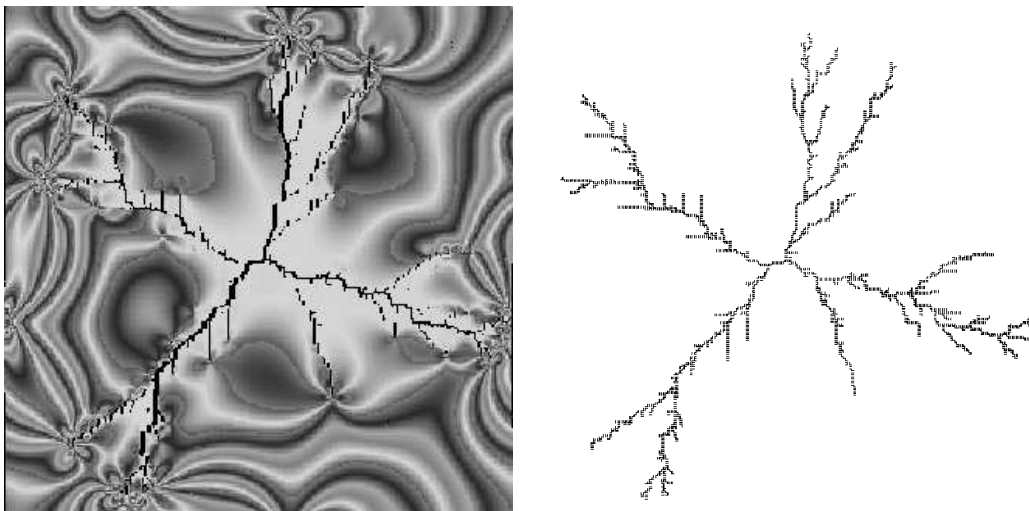


Figure 8: (Left figure): A typical crack obtained with a beam model for hydraulic fracturing at constant pressure, on a square lattice of 250×250 with periodic boundary conditions. All beams under tension break with the same probability. The crack consists of 2200 broken beams. The greyscale represents the difference of the diagonal elements of the hydrostatic stress field. (Right figure): Only the crack structure.³⁵

solution. The corresponding structures are usually spatially compact.

It is important to note that the growth rule and in particular the employed growth exponent η is completely independent of the investigated field equation. Rather the growth rule bases on plausible considerations.

There has been subsequently work been done to apply stochastic growth rules onto elastic systems, especially applying them to crack growth problems. The “Gradient” in the growth rule is then typically replaced by the hydrostatic strain (eigenvalue) component. For certain classes of tensile problems fractal crack growth was found on two dimensional Hookean spring networks, exhibiting a fractal dimension $d_f \approx 1.6$ for $\eta = 1$.^{21,22,23} This value for d_f is relatively close to the one observed in a DLA problem. However, the first author of this review conducted simulations on two dimensional beam lattices (see Sec.2.2) where a small preexisting crack was loaded at constant pressure from inside, and found non-fractal rather compact crack growth, already for $\eta = 1$.¹⁵ It was concluded that compressed microstructural elements (beams) should not be considered for the breaking process because of the very asymmetry of interatomic potentials. With this modified breaking rule also non-fractal cracks were found for $\eta = 1$. The cracks were, however, now linear in shape. In order to obtain in a hydraulic fracture simulation persisting branching cracks, much stronger fluctuations need to occur than obtainable with $\eta = 1$. This is not so surprising as almost the

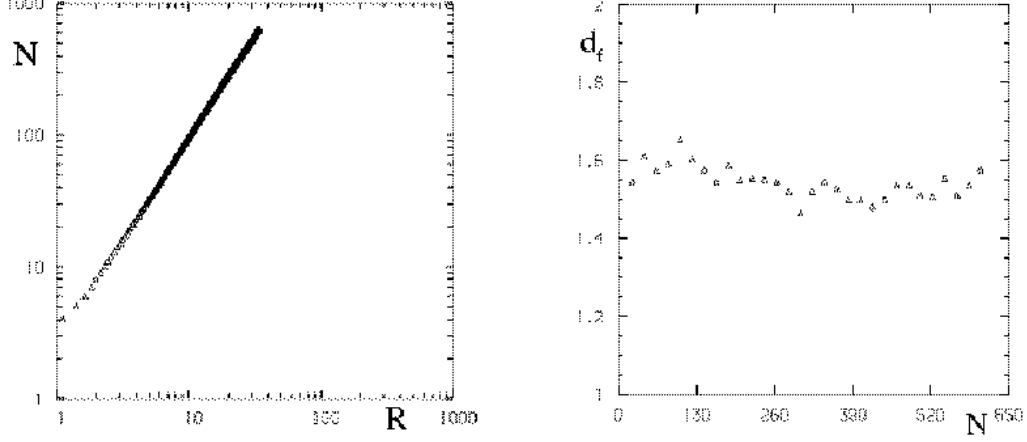


Figure 9: (Left figure): Double-logarithmic plot of the number of broken beams N as a function of the average crack radius R for free boundary conditions. Note the power-law behavior, $N \sim R^{d_f}$, indicating fractal crack growth. (Right figure): Plot of the successive slopes d_f of the data, indicating an average value for the fractal dimension $d_f = 1.56 \pm 0.05$.¹⁵

whole elastic bulk is in a compressed state, while just around the crack tips there exist very narrow cones of elements being in a stretched state. In Fig. 8 we show the crack of a single, very large simulation for the case of maximum fluctuations, i.e., $\eta = 0$ using the above mentioned asymmetric breaking criterion. Note that the breaking probability does *not* depend on the strain magnitude, however, all compressed beams are assigned a breaking probability identically to zero. The hydraulic pressure inside the crack was kept constant and the external boundaries are periodic in displacements, i.e., spanned on a torus. Furthermore the system is assumed as impermeable and there are no losses of the hydraulic fluid. The resulting crack structures are scaleinvariant (fractal) as can be seen in Fig.9. The measured fractal dimension $d_f = 1.56 \pm 0.05$ is slightly below the numerical value for tensile problems, and slightly above the experimental value $d_f = 1.41$ obtained from hydraulic fracturing of clay pastes in two dimensions, compare Fig.3.

The total crack opening volume of the ramified cracks has been calculated and monitored during the growth, and plotted versa the average crack radius. This is shown in Fig.10. The crack opening volume for fractal cracks shows the same dependency on (average) cracks size in comparison to straight cracks, namely $V \sim R^2$.

We note that the foregoing considerations and results are for *impermeable* elastic materials, i.e., the influence of possible effects due to hydraulic fluid flow (hydraulic losses) have been neglected.

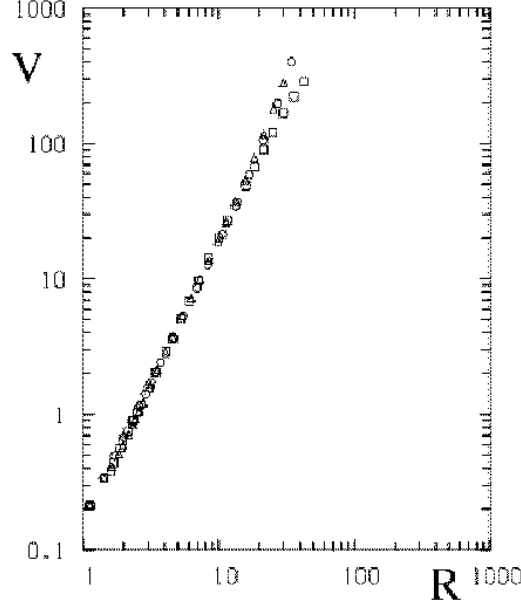


Figure 10: Plot of the crack opening volume V as a function of the average crack radius R for fractal cracks with dimension $d_f = 1.56$ using (\triangle) free boundary conditions and (\square) periodic boundary conditions. For comparison we show also results for a straight crack (\circ) employing free boundary conditions. In all three cases we find the behavior $V \sim R^2$ (in $d = 2$).¹⁵

5 Hydraulic Fracturing with structural disorder

The concept of a local cohesion strength has been used in a number of papers.¹⁹ One assumes that a deformed elastic element connecting sites i and j breaks above a certain material specific threshold force F_{th}^{ij} ('cohesion strength'). This kind of disorder is also called deterministic or quenched disorder in the literature, because once the breaking thresholds have been chosen the model behaves in a completely deterministic way, contrary to the model described in the foregoing section. However, we prefer the term 'structural disorder' as a spatial variation in material properties is frequently associated with certain micro-structural particularities within a material. If the inner stresses are above their thresholds the beams are broken and removed, i.e. their elastic moduli are set to zero. Since the cohesive strength for compression is much higher than for tension we assume that compressed beams cannot break.¹⁵ The breaking thresholds are initially distributed randomly according to some probability density function, $\rho(F_{th})$. At this point it would be ideal to employ empirical strength distributions of the considered material for $\rho(F_{th})$. However, at the present stage of research we are basically interested in generic features of such crack growth models. The

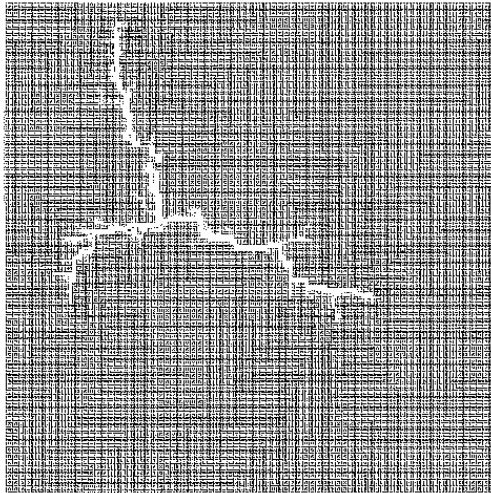


Figure 11: Typical hydraulic crack for strong disorder, $r = -0.7$ and $\langle F_{th} \rangle = 0.01$, on a lattice of size $L = 150$. The crack consists of 629 broken beams after 1500 time steps using a hydraulic flux $q_{in} = 0.05$. The injection point is the center of the lattice. We have used periodic boundary conditions in vertical and horizontal directions.¹⁶

width of the strength distribution is most easily controlled employing power-law distributions,

$$\rho(F_{th}) \sim F_{th}^r, \quad (20)$$

with $F_{th} \in [0, F_{max}]$ and $r > -1$. Negative exponents r are used to describe strong cohesive disorder (broad distributions) while large positive exponents correspond to weak disorder (narrow distributions). It is convenient to express the normalization factor and F_{max} by the distribution's expectation value $\langle F_{th} \rangle$ and the exponent r . This allows to investigate disorder effects due to deviations around $\langle F_{th} \rangle$ for constant $\langle F_{th} \rangle$.

In the following we will discuss the modelling of crack growth in impermeable and permeable materials separately because the employed breaking criteria slightly differ for both cases.

5.1 The impermeable medium

The hydraulic fracturing of an impermeable solid represents a limiting case due to the vanishing hydraulic losses. For a porous material saturated by an incompressible fluid this would imply that *only* pure shear deformations would be possible. This follows directly from the time-dependent flow equation, i.e., for $k \rightarrow 0$ or $\mu \rightarrow \infty$ Eq. (5) reduces to the condition $\text{div} \mathbf{u} = \text{const.}$ preserving the volume of a deformation. This is not a very typical experimental situation. However, if the

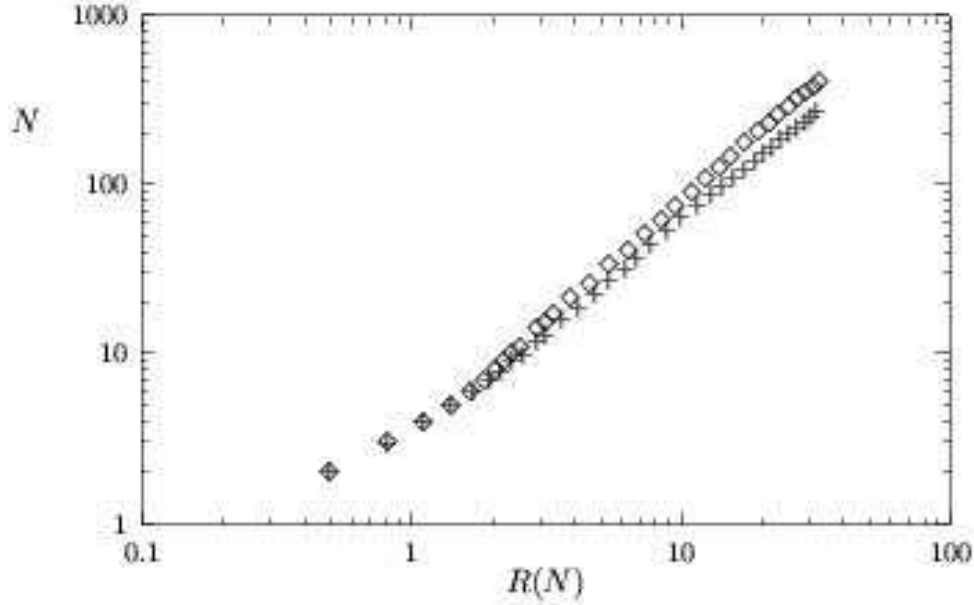


Figure 12: Log-log plot of the number N of broken beams versus the average radius $R(N)$ for two different distributions of breaking thresholds: (\diamond) $r = -0.7$, averages over 60 cracks, fractal dimension $d_f = 1.44 \pm 0.10$; (+) $r = -0.5$, averages over 53 cracks, fractal dimension $d_f = 1.39 \pm 0.10$. For all simulations we have used an average cohesion value $\langle F_{th} \rangle = 0.01$ and a linear lattice size $L = 150$.¹⁶

pores are filled by very compressible gases one might even neglect the deformation dependent volume forces for impermeable solids.

In the following we consider the case where an incompressible fluid hydraulically propagates a crack through an impermeable material. We require that the pores are filled by a very compressible substance compared to the solids compressibility. Such situation is approximately encountered for magma driven cracks.³⁶

We consider a constant fluid injection rate, $q_{in} = 5 \cdot 10^{-2} l^2 d$, into the hydraulic crack and a vanishing pore pressure, $p_0 = 0$. The boundary conditions have been discussed in Sec. 2.4, i.e., see Eq. (11) for vanishing Darcy losses, $D^* = 0$. The simulation procedure follows the mentioned steps 1-9 in Sec. 2.4 with the exception that in the present case no pressure equations need to be solved. Instead the ‘test pressure’ p^* does appear directly as inhomogeneity for the elastic equations along the crack contour. Initially one small crack (one broken vertical beam) is prepared on the grid center. For the distribution of breaking thresholds, Eq. (20), the values $\langle F_{th} \rangle = 10^{-2}$ (arbitrary units), $r = -0.5$ and $r = -0.7$ (strong disorder), and $r = +\infty$ (no disorder) are used. After each time increment, $\Delta t = 1$, all beams carrying *tensile* forces larger than the associated breaking

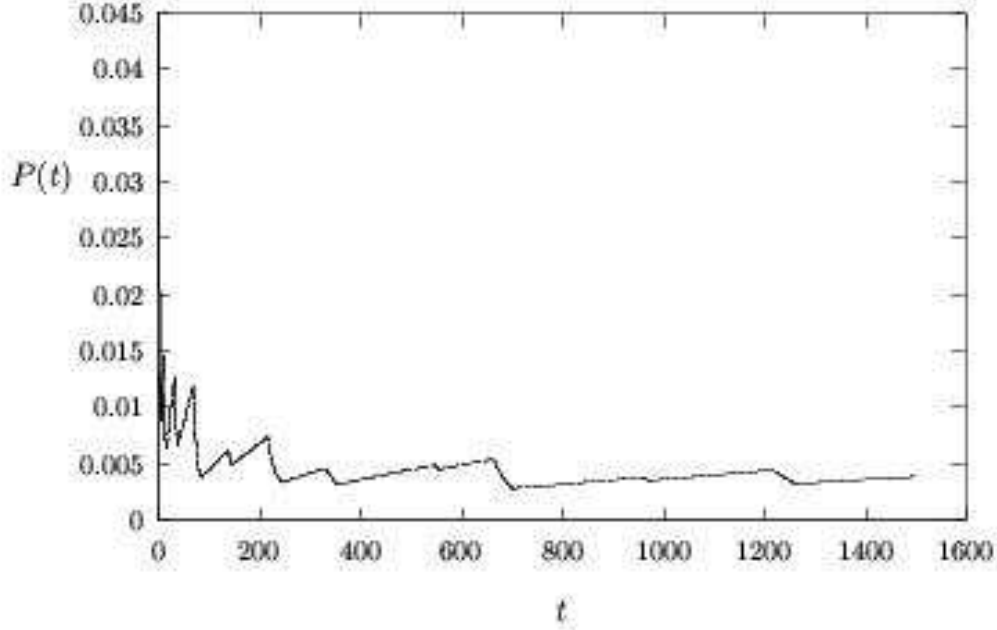


Figure 13: Linear plot of the pressure P inside the crack versus time t . The record corresponds to the simulation displayed in Fig. 11.¹⁶

thresholds are broken, i.e., their elastic moduli are set to zero.

For $r = +\infty$ (no disorder) straight cracks are observed and the hydraulic crack pressure drops in form of a power-law in time, $P(t) \sim t^{-1/3}$.¹⁶

For strong disorder the situation becomes more complicated. In Fig. 11 we show a calculated sample crack. The obtained crack is a branching structure exhibiting many small scale branches but only a very few branches on the larger length scale. A comparison with the crack structure shown in Fig. 8 reveals a much lower crack density in the present case. This is directly measured in Fig. 12 by plotting the number of broken beams N in dependence of the average crack size R ,³⁷ yielding the cracks fractal dimension d_f using the relationship $N \sim R^{d_f}$. The fractal dimensions for the investigated threshold distributions $r = -0.7$ (\diamond) and $r = -0.5$ ($+$) take the values $d_f = 1.44 \pm 0.10$ and $d_f = 1.39 \pm 0.10$ respectively. These values for d_f are consistent with the fractal dimension found in the two dimensional experiments on hydraulic fracturing of viscoelastic clays.¹⁰

The time record of the hydraulic pressure at the injection point is of considerable interest because on the one hand it is often experimentally measurable and on the other hand does it contain information about rheological and breaking properties. If the considered crack is at rest the hydraulic pressure P will generally build up in time (loading). For an impermeable medium the pressure build up will correspond to the materials elastic response on the injected fluid

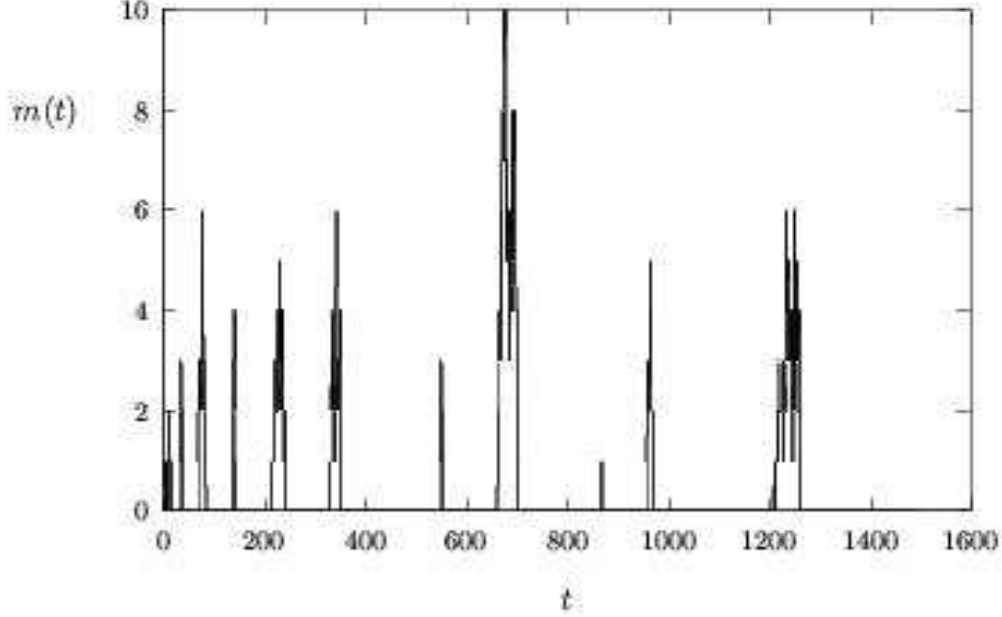


Figure 14: Temporal breaking sequence corresponding to the crack displayed in Fig. 11. The magnitude $m(t)$ is defined as the number of per unit time step simultaneously broken beams. The simulation was stopped after 1500 time steps. Note the clustering of breaking events and the large time intervals of quiescence.¹⁶

(and possible fluid flow effects within the crack which are neglect in the present case). We consider the fluid as incompressible implying a linear relationship between crack volume and time, and due to the linearity and time independence of employed elastic equations a linear increase of pressure in time is the consequence. The associated slope is related to the materials mechanical stiffness (for the present crack). However, if the crack starts to move the stiffness decreases and so does the hydraulic pressure. There exists a cutoff for this pressure drop because the materials average cohesion is non-zero. Therefore the crack comes to rest again after some time period. Figure 13 displays such an ‘erratic’ pressure record. The strongest pressure fluctuations occur for small cracks (early times) at high frequency whereas lateron the loading periods become larger and larger. This is due to the rapidly decreasing stiffness as soon as the crack advances. The loading periods are periods of ‘quiescence’ (no breaking); the unloading periods correspond to ‘bursts’ (temporally localized groups of breaking events). This is exemplified in Fig. 14. The temporal correlations of such bursts have been analyzed in detail in Ref. 16.

5.2 The permeable medium

This section considers hydro-fracturing of a permeable porous medium, where an incompressible fluid is injected at the center of a quadratic grid at a constant rate, q_{in} . The boundary conditions have been discussed in Sec. 2.4.

The dimensionless formulation of the pressure equation is first explained before we show some examples. The considered pressure equation Eq. (6) is made dimensionless by considering the forces acting on the beams surrounding the injection cell at the center of the grid. Darcy's law yields the Darcy velocity $v = -(k/\mu)dp/dx$ in the x -direction. The Darcy velocity is also v in the y -direction when assuming symmetry. The forces acting on the beams surrounding the injection cell are $F = l^2 d dp/dx$, because the pressure difference between two neighbor cells is $dp = (dp/dx)l$. The length of a beam is l and the width of a beam is d . The beam force F can be written $F = \mu v l^2 d/k$, when Darcy's law is used to replace the pressure gradient dp/dx with the Darcy velocity v . The volume flux into the center cell is initially $q_{in} = v l^2$. The force F is written in terms of q_{in} rather than v , and we have $F = \mu q_{in} d/k$. This force is scaled with the unit force $F_0 = E d^2$, (where E is Young's modulus), which can be written $F/F_0 = q_{in}/q_0$. The unit injection rate becomes $q_0 = k E d/\mu$.

This scaling shows two things. Firstly, it shows that a dimensionless injection rate of order one or larger implies strong enough forces on the center cell for deformations on grid to be noticeable. Secondly, the (dimensionless) average beam strength must be less than q_{in}/q_0 for a crack to nucleate.

The characteristic time becomes $t_0 = \mu l^2/(E k)$, which will be as low as nano seconds for a grid with beam length $l = 10^{-5}$ m, permeability $k \sim 10^{-15}$ m², Young's modulus $E \sim 10^{11}$ Pa, and fluid viscosity $\mu \sim 10^{-3}$ Pa s. We consider a constant permeability throughout the material.

The full pressure equation for an incompressible fluid Eq. (5) is not solved. The pressure equation is therefore not fully coupled to the volume changes in both the bulk and the fracture. However, it is still possible to couple the hydraulic pressure to the elastic deformations of the crack by considering conservation of fluid, as shown in Sec. 2.4. The (Laplacian) pressure equation is first solved for a unit pressure p^* on the crack contour. The total Darcy flux D^* is determined from this solution; the corresponding crack volume V^* is computed from the associated elastic solution. The scaling parameter $\lambda(t)$ yielding the physical pressures and strains is computed each time step according Eq. (11), see Sec. 2.4 steps 1-9.

The beams on the crack surface are checked after each time step to see if any of them are stretched beyond their strength. If there are any over-stretched beams, then the most over-stretched beam will be broken. We showed in the foregoing section that the advance of fracture is localized in time in form of bursts, separated by large time periods of quiescence (loading). The time-step used during the bursts is therefore "small". On the other hand, the quiet periods

Case	Average beam strength	Injection rate
No	$\langle F_{th} \rangle / F_0$	q_{in} / q_0
I	10^{-2}	10^{-3}
II	10^{-3}	10^{-3}
III	10^{-4}	10^{-3}

Table 1: The numerical cases have the same injection rate q_{in} , but differ for the average beam strength $\langle F_{th} \rangle$.

between two bursts can be very long compared to the short time span of a burst. The time-step is therefore multiplied by a factor larger than 1 after time-steps where no beams were broken. This factor could be chosen so that ten such steps together yield a combined factor equal to for instance 2 or 10. Increasing each time-step between the bursts by a factor makes it possible to obtain a step length sufficiently long to get through these relatively long periods of pressure build-up. However, the time-step is immediately set to its minimum value once a new beam breaks.

Three numerical examples are studied, which differ in the average beam strength $\langle F_{th} \rangle$. The average beam strength in these cases and the injection rate q_{in} are given in the Table 1. All three cases have the grid size 100×100 and a beam strength distribution characterized by the exponent $r = -0.9$, compare Eq. (20).

A value for r close to -1 indicates that the beams have very broadly distributed strengths. The employed material and geometry dependent constants are $a = 1$, $b = 2.5$ and $c = 1200$, when expressed dimensionless. (The scaling of these constants is such that a becomes 1.)

The crack in case I, where $q_{in}/q_0 \ll \langle F_{th} \rangle / F_0$, is shown in Fig. 15a. This figure shows the crack after it stopped growing. The hydraulic pressure is shown in Fig. 15b, where it is seen that the pressure reaches a stationary value. A small crack nucleated in this case, even though the average beam strength is 10 times larger than the injection rate. This is due to the strong heterogeneities ($r = -0.9$). The pressure follows an exponential rise in time according to the expression for the scaling parameter λ in Eq. (9). The first smooth rise of the pressure ends by breaking beams until no more beams are overstressed, and a second rise of pressure follows. This second rise leads to a stationary pressure. Notice that the first rise of pressure points towards a higher stationary pressure than the second rise. This is expected because the maximum possible pressure in a constant crack geometry, given a constant injection rate, is decreasing with increasing crack size. A large crack requires a lower stationary hydraulic pressure compared to a small crack in order to balance the injection rate to the hydraulic losses. The small crack seen in Fig. 15a is almost entirely due to the first burst. After the first burst, the

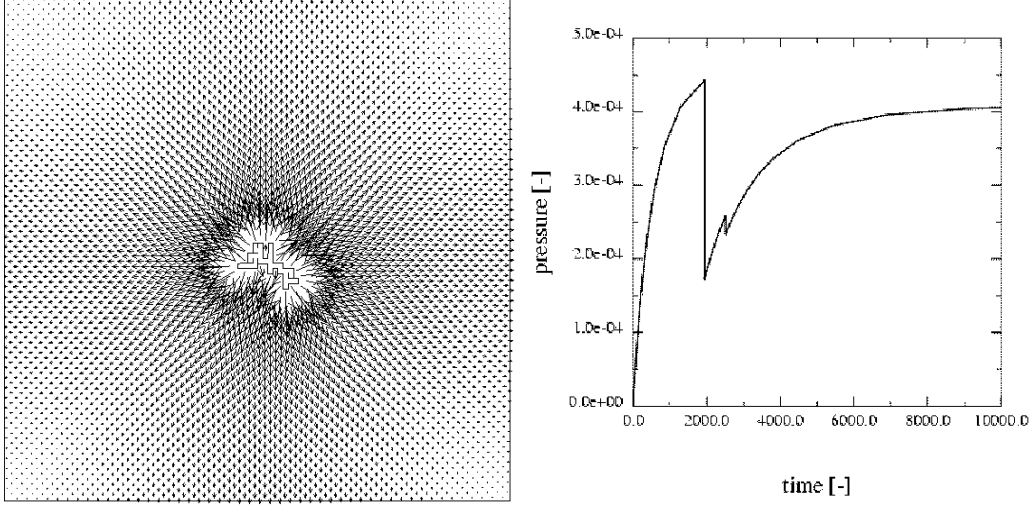


Figure 15: Case I has an average beam strength $\langle F_{th} \rangle / F_0 = 10^{-2}$ and an injection rate $q_{in}/q_0 = 10^{-3}$. (a) (left) The final state of the branching crack structure and the corresponding Darcy flow field. (b) (right) The hydraulic pressure in the crack as a function of time.¹⁷

pressure cannot reach a sufficiently high level any more to break more beams. The time τ (see Eq. (10)) is plotted in Fig. 18a. Because τ measures the typical elastic response versus the typical flow response, it defines the characteristic time scale below which the (re)loading process appears to happen within an impermeable medium. It is seen that τ is increasing in crack size, which is consistent with the pressure plot Fig. 15b. The characteristic time increases with the crack size even though the stationary pressure is decreasing.

The case II shows crack propagation for an average beam strength equal to the injection rate, see Table 1. The forces from the fluid gradients on the beam structure are then comparable with the strength of the beams. The pressure during the cracking process is shown in Fig. 16b, and it is seen that the pressure is rising almost linearly between the bursts of beam breaking. The small initial bursts were sufficient to generate a crack with a time constant τ much larger than the time span shown in the pressure plot. This explains why the pressure rise appears almost linear rather than exponential in time as given by Eq. (9). The characteristic time τ is shown in Fig. 18b. The crack structure at the end of the time period in the pressure plot (Fig. 16b) is shown in Fig. 16a. The crack in this case of broadly distributed beam strengths shows the growth of a branching crack structure. Note that within the crack ‘fjords’ the Darcy flow almost vanishes.

Case III has an average beam strengths $\langle F_{th} \rangle / F_0$ one order of magnitude lower than the injection rate q_{in}/q_0 . The injection rate is therefore high compared to strength of the structure. This is also seen from the pressure plot in Fig. 17b,

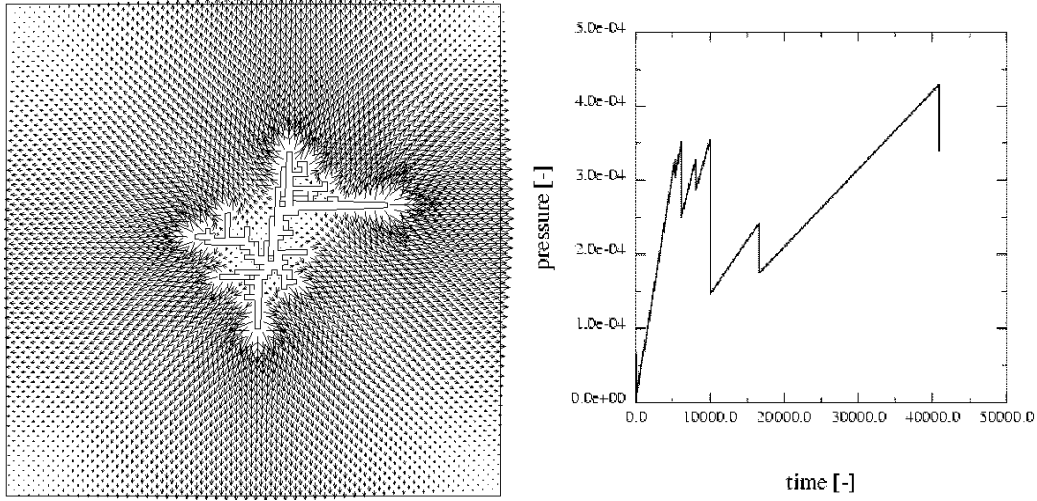


Figure 16: Case II has an average beam strength $\langle F_{th} \rangle / F_0 = 10^{-3}$ and an injection rate $q_{in}/q_0 = 10^{-3}$. (a) (left) The crack and the corresponding Darcy flow field. (b) (right) The hydraulic pressure in the crack as a function of time.¹⁷

which is characterized by more frequent bursts compared to case II. Only a slight pressure increase is enough to trigger a new burst. The hydraulic pressure level of beam breaking in Fig. 17b is about one order of magnitude lower than the corresponding pressure level in figure Fig. 16b. This is as expected from the average beam strengths of these cases. The characteristic time τ for case III is shown in Fig. 18c, which also shows a large number of bursts. The crack in its final state is shown in Fig. 17a. A branching crack structure is seen, where the branch close to the boundary seems to be growing faster than the other branches. This seems to be a boundary effect because the pressure gradients close to a boundary are larger. This effect favours growth of cracks close to the boundaries.

The presented cases demonstrate several features of hydraulic fracturing in a permeable medium with broadly distributed cohesion, when a fluid is injected at a constant rate at the center of the test sample. They clearly show how the hydraulic pressure is increasing during “quiet” periods. The pressure increases according to Eq. (9). The characteristic time τ in Eq. (10) is computed, and it is seen that τ becomes large compared to the time period between successive bursts. The pressure therefore appears to rise linearly between the bursts. The characteristic time τ is also increasing with the crack size, which implies that the time periods between successive bursts get longer as the crack grows. This can also be seen from the slopes in Figs. 15b-17b which are decreasing with increasing crack size. The pressure drops during the bursts. Furthermore, the bursts also become more frequent when the average beam strength $\langle F_{th} \rangle / F_0$ gets low

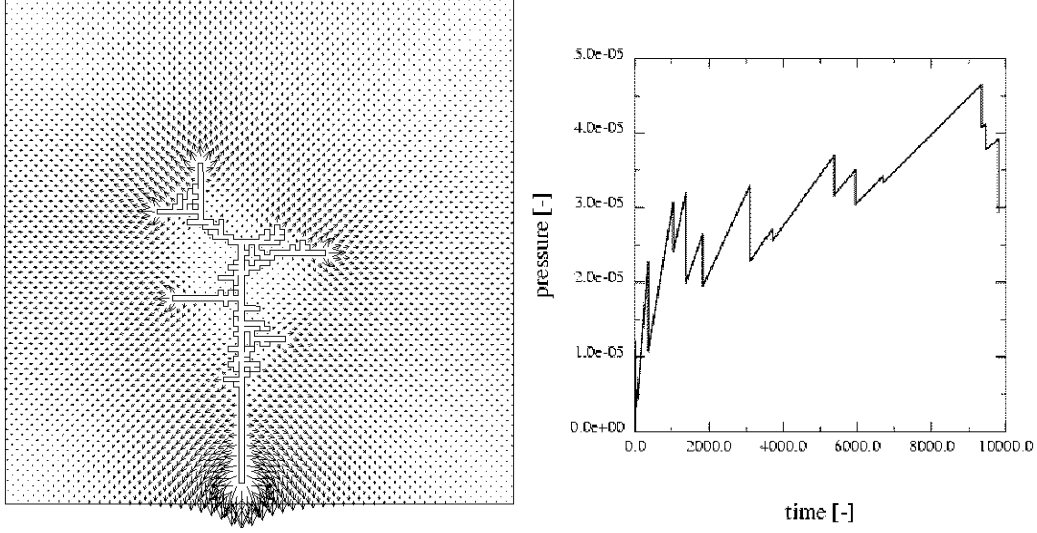


Figure 17: Case III has an average beam strength $\langle F_{th} \rangle / F_0 = 10^{-4}$ and an injection rate $q_{in}/q_0 = 10^{-3}$. (a) (left) The crack and the corresponding flow field. Note the screening of the flow field within the crack branches. (b) (right) The hydraulic pressure in the crack as a function of time.¹⁷

compared to the injection rate q_{in}/q_0 .

Conclusion

We have reviewed some numerical results for hydraulic fracturing in porous materials employing microstructural fracture growth models. The considered models are *not* finite difference schemes of certain continuum mechanical equations. Rather they implement an approach to crack growth problems in the spirit of Monte Carlo methods of statistical mechanics. This allows to track quasistatic crack growth under very general conditions, i.e., for disordered systems on mesoscopic length scales.

Acknowledgments

F. T. would like to acknowledge financial support from CEC under grant number ERBFMBICT 950009.

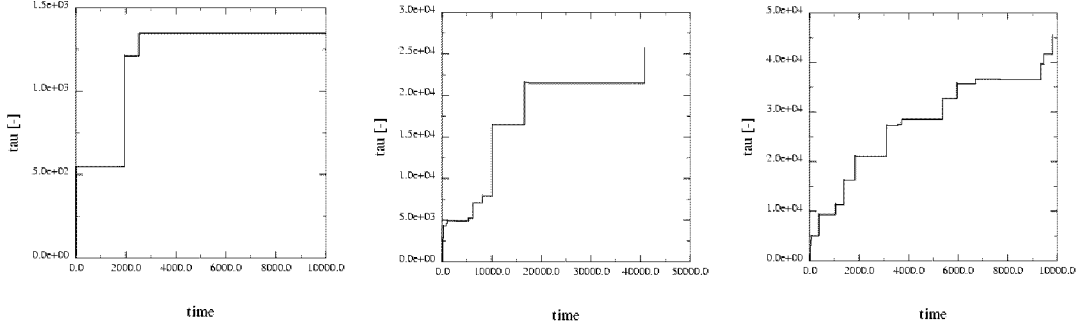


Figure 18: The characteristic time $\tau = \int \mathbf{u}^* \cdot d\mathbf{A} / \int \mathbf{v}^* \cdot d\mathbf{A}$ as a function of crack growth for the three cases of Table 1.

References

- [1] Griffith, A.A. The phenomena of rupture and flow in solids, *Phil. Trans. Roy. Soc. London*, **A 221**, pp. 163-98, 1921.
- [2] Lawn, B. *Fracture of Brittle Solids*, University Press, Cambridge, 1995.
- [3] Chaikin P.M. & Lubensky T.C., *Principles of condensed matter physics*, University Press, Cambridge, 1995.
- [4] Witten, T.A. & Sander, L.M. Diffusion-limited aggregation, a kinetic critical phenomenon, *Phys. Rev. Lett.*, **47**, pp. 1400-3, 1981. Pietronero, L. & Wiesmann, H.J. From physical dielectric breakdown to the stochastic fractal model, *Z. Phys.*, **B 70**, pp. 87-93, 1988.
- [5] Feder J. *Fractals*, Plenum Press, New York and London, 1989.
- [6] Bunde, A. & Havlin, S. (eds) *Fractals and Disordered Systems*, Springer, Berlin Heidelberg, 1991.
- [7] Vicsek T. *Fractal Growth Phenomena*, World Scientific, Singapore, 1989.
- [8] Kessler, D.A. & Koplik, J. & Levine, H. Pattern selection in fingered growth phenomena, *Adv. Phys.*, **37**, pp. 255-336, 1988.
- [9] Schwörer, F. *Phys. Bl.*, **41**, pp. 142, 1985.
- [10] Van Damme, H. & Lemaire, E. From flow to fracture and fragmentation in colloidal media in *Disorder and Fracture*, Charmet J.C. (ed), Plenum Press, New York, pp. 83-104, 1990.
- [11] Biot, M.A. General theory of three-dimensional consolidation, *J. Appl. Phys.*, **12**, pp. 155-64, 1941.

- [12] The dual lattice of a square lattice is also a square lattice, however, displaced half a lattice constant both in x and y directions ($d = 2$).
- [13] Herrmann, H.J. & Roux, S. (eds.), *Statistical Models for the Fracture of Disordered Media*, pp. 232, North Holland, Amsterdam, 1990.
- [14] Boley, B.A. & Weiner, J.H. *Theory of Thermal Stresses*, pp. 243, Dover, New York, 1960.
- [15] Tzschichholz, F., Herrmann, H.J., Roman, H.E. & Pfuff M. Beam model for hydraulic fracturing, *Phys. Rev.*, **B 49**, pp. 7056-9, 1994.
- [16] Tzschichholz, F. & Herrmann, H.J. Simulations of pressure fluctuations and acoustic emission in hydraulic fracturing, *Phys. Rev.*, **E 51**, pp. 1961-70, 1995.
- [17] Wangen, M. & Tzschichholz, F. (in preparation).
- [18] Tzschichholz, F. Fracturing of brittle homogeneous solids: Finite-size scalings, *Phys. Rev.*, **B 52**, pp. 9270-4, 1995.
- [19] Roux, S. & Hansen, A. & Herrmann, H.J. & Guyon, E. Rupture of heterogeneous media in the limit of infinite disorder, *J. Stat. Phys.*, **52**, pp. 251-8, 1988; Herrmann, H.J. & Hansen, A. & Roux, S. Fracture of disordered, elastic lattices in two dimensions, *Phys. Rev.*, **B 39**, pp. 637-48, 1989; de Arcangelis, L. & Herrmann, H.J. Scaling and multiscaling laws in random fuse networks, *Phys. Rev.*, **B 39**, pp. 2678-84, 1989.
- [20] de Arcangelis, L. & Redner, S. & Herrmann, H.J. A random fuse model for breaking processes, *J. Phys. (Paris) Lett.*, **46**, pp. L585-90, 1985.
- [21] Louis, E. & Guinea, F. The fractal nature of fracture, *Europhys. Lett.*, **3**, pp. 871-7, 1987.
- [22] Meakin, P. & Li, G. & Sander, L.M. A simple two-dimensional model for crack propagation, *J. Phys.*, **A 22**, pp. 1393-404, 1989.
- [23] Hinrichsen, E.L. & Hansen, A. & Roux, S. A fracture growth model, *Europhys. Lett.*, **8**, pp. 1-7, 1989.
- [24] de Arcangelis, L. & Hansen, A. & Herrmann, H.J. & Roux, S. Scaling laws in fracture, *Phys. Rev.*, **B 40**, pp. 877-80, 1989.
- [25] Kahng, B. & Batrouni, G.G. & Redner, S. & de Arcangelis, L. & Herrmann, H.J. Electrical breakdown in a fuse network with random, continuously distributed breaking strengths, *Phys. Rev.*, **B 37**, pp. 7625-37, 1988.

- [26] Takahashi, H. & Abé, H. in *Fracture Mechanics of Rock* pp. 241-76, ed. B.K. Atkinson, Academic Press, London, 1987.
- [27] Batrouni, G.G. & Hansen, A. Fourier acceleration of iterative processes in disordered systems, *J. Stat. Phys.*, **52**, pp. 747-73, 1988.
- [28] Hahn H.G. *Bruchmechanik*, Teubner, Stuttgart, 1976.
- [29] Sneddon, I. & Lowengrub, M. *Crack problems in the classical theory of elasticity*, SIAM, Philadelphia, 1969.
- [30] Muskhelishvili N.I. *Some basic problems of the mathematical theory of elasticity*, P. Nordhoff, Groningen, 1953.
- [31] Making the transition from an atomistic lattice theory to a simple continuum theory one drops in fact the mentioned gradient terms, mainly because of the ‘infinitesimal’ atomic equilibrium spacings [See for example: Leibfried, G. & Breuer, N. *Point Defects in Metals I*, Springer, Berlin Heidelberg New York, 1978]. However, mesoscopic lattice models do always exhibit higher order gradient terms as compared to unstructured continua.
- [32] Truesdell, C.A. & Toupin, R.A. *Encyclopedia of Physics*, Vol. III/I, Flügge S. (ed), Springer, Berlin Göttingen Heidelberg, 1960; Toupin, R.A. Elastic materials with couple-stresses, *Arch. Rat. Mech. Anal.* **11**, pp. 385-414, 1962; Green, A.E. & Rivlin, R.S. Simple force and stress multipoles. (Simple force and stress multipole theory for distributed surface and body forces), *Arch. Rat. Mech. Anal.* **16**, pp. 325-53, 1964.
- [33] Altan, S.B. & Aifantis, E.C. On the structure of mode III crack-tip in gradient elasticity, *Scripta Metallurgica et Materialia*, **26**, pp. 319-24, 1992.
- [34] Westergaard, H.M. Bearing pressures and cracks, *Journal of Applied Mechanics*, **6**, pp. 49-53, 1939.
- [35] Herrmann, H.J. & Poliakov, A.N.B. & Tzschichholz, F. The Deformation of Rocks: Fractals everywhere, *Fractals*, **3**, pp. 821-8, 1995.
- [36] Spence, D.A. & Turcotte, D.L. Magma-Driven Propagation of Cracks, *J. Geophys. Res.*, **90**, pp. 575-80, 1985.
- [37] The typical radius R of a branching crack structure is preferably calculated as a radius of gyration, $R^2(N) = \frac{1}{N} \sum_i (\vec{r}_i - \vec{r}_0)^2$ with $\vec{r}_0 = \frac{1}{N} \sum_i \vec{r}_i$.